DISTRIBUTION STATEMENT A. Approved for public release; distribution is unlimited.

Biological Response to the Dynamic Spectral-Polarized Underwater Light Field

PI: Molly E. Cummings
Section of Integrative Biology C0930
University of Texas
Austin, TX 78712
phone: (512) 471-5162 fax: (512) 471-3878 email: mcummings@mail.utexas.edu

Co-PI: Samir Ahmed (City College of New York)
Co-PI: Heidi Dierssen (University of Connecticut)
Co-PI: Alexander Gilerson (City College of New York)
Co-PI: William F. Gilly (Stanford University)
Co-PI: George Kattawar (Texas A & M University)
Co-PI: Brad Seibel (University of Rhode Island)
Co-PI: James Sullivan (University of Rhode Island)

Award Number: N000140911054
http://www.bio.utexas.edu/research/cummingslab/

LONG-TERM GOALS

Camouflage in marine environments requires matching all of the background optical properties: spectral, intensity and polarization components─ all of which can change dynamically in space and time. Current research suggests that polarization detection is more sensitive than other conventional detection methods in scattering media such as the ocean, hence underscoring the need to develop polarized camouflage technology. Our research investigates the biological challenge of camouflage in the near-shore littoral zone and near-surface marine environments in two distinct water types found in coastal environments around the globe (oligotrophic and eutrophic) with particular emphasis on the polarization properties. We aim to characterize the dynamic light field along with the behavioral and cellular response of camouflaging animals in these environments. Our long-term goal is to identify the biological pathways for concealment against the underwater spectral-polarized light field enabling us to identify design principles for future naval camouflage.

OBJECTIVES

(1) Measure and model the spectral-polarized light field in near-shore and near-surface environments

(2) Characterize the biological camouflage response of organisms to these dynamic optical fields

(3) Identify the internal controls and structural mechanisms that coordinate the camouflage response

Report Documentation Page

Form Approved
OMB No. 0704-0188

Public reporting burden for the collection of information is estimated to average 1 hour per response, including the time for reviewing instructions, searching existing data sources, gathering and maintaining the data needed, and completing and reviewing the collection of information. Send comments regarding this burden estimate or any other aspect of this collection of information, including suggestions for reducing this burden, to Washington Headquarters Services, Directorate for Information Operations and Reports, 1215 Jefferson Davis Highway, Suite 1204, Arlington VA 22202-4302. Respondents should be aware that notwithstanding any other provision of law, no person shall be subject to a penalty for failing to comply with a collection of information if it does not display a currently valid OMB control number.

1. REPORT DATE	2. REPORT TYPE	3. DATES COVERED
30 SEP 2011		**00-00-2011 to 00-00-2011**

4. TITLE AND SUBTITLE	5a. CONTRACT NUMBER
Biological Response to the Dynamic Spectral-Polarized Underwater Light Field	5b. GRANT NUMBER
	5c. PROGRAM ELEMENT NUMBER
6. AUTHOR(S)	5d. PROJECT NUMBER
	5e. TASK NUMBER
	5f. WORK UNIT NUMBER
7. PERFORMING ORGANIZATION NAME(S) AND ADDRESS(ES) **University of Texas,Section of Integrative Biology C0930,Austin,TX,78712**	8. PERFORMING ORGANIZATION REPORT NUMBER
9. SPONSORING/MONITORING AGENCY NAME(S) AND ADDRESS(ES)	10. SPONSOR/MONITOR'S ACRONYM(S)
	11. SPONSOR/MONITOR'S REPORT NUMBER(S)

12. DISTRIBUTION/AVAILABILITY STATEMENT
Approved for public release; distribution unlimited

13. SUPPLEMENTARY NOTES

14. ABSTRACT

15. SUBJECT TERMS

16. SECURITY CLASSIFICATION OF:			17. LIMITATION OF ABSTRACT	18. NUMBER OF PAGES	19a. NAME OF RESPONSIBLE PERSON
a. REPORT	b. ABSTRACT	c. THIS PAGE			
unclassified	**unclassified**	**unclassified**	**Same as Report (SAR)**	**20**	

APPROACH

Our first aim is to **measure and model the underwater spectral-polarized light field in distinct water types** (oligotrophic and eutrophic). The spectral-polarized light field will be measured by the simultaneous deployment of a comprehensive optical suite including underwater video-polarimetry (Cummings), inherent optical properties, (LISST by Dierssen), hyper-spectral multi-angular Stokes vector spectroradiometry (Gilerson and Ahmed), and the volume scattering function measures (MASCOT by Sullivan). These measurements will be used to refine development of, and make comparisons to, theoretical expectations from a fully 3-D radiative transfer model that solves for each of the polarization elements of the Mueller matrix transformation of the Stokes vector by (Kattawar), as well as to set boundary conditions for laboratory experiments.

The first modeling objective of this proposal is to calculate the complete Mueller matrix/Stokes vector for any set of oceanic and atmospheric conditions for any region of the ocean. We will then use this modeling approach (*i*) to predict the 3-D light field; (*ii*) to calculate experimental conditions to measure biological responses; and (*iii*) to investigate the nature of the light field as it interacts with cells within the skin. Our approach is to modify the 1D Monte Carlo codes of Kattawar (1) and the RayXP code of Zege (2) to develop a 3-D Monte Carlo model with full Mueller matrix treatment.

Our second objective is to **quantify the biological response to these dynamic optical environments** by field observations and laboratory measurements of vertebrate and invertebrate animals. For this second objective, we will quantify background matching of animals in their native near-shore and near-surface environments using a diver-operated video polarimeter (Cummings), and also in a laboratory setting that allows us to recreate and manipulate optical measurements recorded in the field (Cummings, Dierssen, Sullivan, Ahmed, Gilerson, Seibel, Kattawar). Specialized experimental tanks that allow for manipulating isolated components of the incident light field (e.g. altering the e-vector orientation without changes in intensity) will be employed to test animal responses. Animal response will be measured using the underwater video polarimeter and hyperspectral imager.

Our third objective is to **identify the internal control and structural mechanisms that coordinate the camouflage response**. Here we plan to provide novel advances in our understanding of camouflage control by (a) examining both iridophore and chromatophore control processes for specific background radiance matching (spectrum and polarization plane) in live, awake animals during the adaptation process (Cummings), (b) thoroughly examining local or peripheral control features (Seibel, Gilly), and (c) developing a novel 3D Monte Carlo model to describe how the spectral-polarized light field interacts with cells within the skin (Kattawar).

Using both field-studied and model organisms, we will employ four approaches: (i) Characterize chromatophore responses to direct electrical stimulation using pharmacological methods to block central control pathways (e.g. blocks axonal sodium channels) to determine local verses peripheral control (Gilly) (*ii*) confocal imagery of live-awake light adapted fish using autofluorescence to identify cell types (Cummings), (*iii*) calcium-imaging optical technique to track the neural control pathway in coordinating a camouflage response in awake animals as well as prepared tissue (Seibel; Gilly; Cummings), (iii) utilize the inherent reflective (iridophores) and pigmentation (melanophores, xanthophores) properties of these cells to characterize real-time response to pharmacological manipulations (norepinephrine, calcium channel blockers, actin/microtubule blockers) as well as manipulations of the input polarization optics (Cummings), (i*v*) identify and characterize peripheral

cell (i.e. skin vs. retinal) opsin expression patterns in ecologically relevant fish species (lookdowns, pinfish) to characterize local sensing mechanism for changes in spectral/polarized light (Cummings). Through these approaches we will characterize the internal control features regulating camouflage in both fish and cephalopods. We will also develop a novel use of Mueller matrix modeling to calculate the interaction of the light field within animal tissues (Kattawar).

WORK COMPLETED

a) Completed 2 field compaigns in Florida Keys (January and August 2011) to measure polarization characteristics with spectral stokes vector radiometry and polarization videoimagery, IOPs and VSF with MASCOT, partical size distributions with LISST, remote sensing reflectance with ASD and HTSRB, and benthic reflectance with DiveSpec in various water environments with impact from different bottoms (Cummings, Gilerson, Sullivan, Twardowski, Dierrsen)

b) Measured camouflaged polarimetry response to live squid and teleost fish in controlled laboratory conditions during field campaigns in Florida to determine dynamic response to changes in the polarized light field (Seibel, Cummings)

c) Presented at Ocean Optics in September 2010 (Cummings, Kattawar, Dierrsen, Gilerson).

d) Participated in annual MURI meeting including field planning meeting in November 2010 at Scripps (Cummings, Dierssen, Kattawar, Sullivan, Gilerson, Ahmed, collaborator Twardowski, Gilly)

e) Integrated CCNY polarimeter with underwater thrusters providing full control of the system azimuth orientation at various depths without help of the divers (Gilerson).

f) Acquired a new full stokes vector video-imaging caera “SALSA” modified for underwater operations, integrated the camera with the polarimeter and thrusters combination for automated control of viewing and azimuth angle measurements. Successfully tested in the field August 2011 (Gilerson).

g) Completed development and implementation of a switching polarizer module (POLMOD) for use with the MASCOT Volume Scattering Function device. The POLMOD automatically controls the polarization of the MASCOT laser output to yield real time measurements of the unpolarized, horizontal, and vertical polarized components of the VSF. Implemented and used for all MURI field work since Jan. 2011 (Sullivan).

h) Began testing a bench-top holographic microscope (HOLOCAM) during MURI field campaigns to conduct holographic particle analysis of field water samples. Results will be compared to SEM analysis of filters from replicate samples to yield estimates of the PSD and TSM (Sullivan).

i) Acquired funding and purchased a hyperspectral imager for use on the project: Surface Optics 710 - USB Visible Hyperspectral Imaging Camera with 400-1000nm spectral range. The imager has been used in a variety of lab and field experiments as outlined below. (Dierssen)

j) Graduate student Brandon Russell participated in a cruise of Gulf of Mexico waters with Sea Education Association. He conducted hyperspectral imaging on live *Sargassum* harvested throughout the region and fish and crabs associated with the floating *Sargassum*. (Dierssen)

k) Conducted experiments at Mystic Aquarium using the submerged imager to measure color camouflage in the winter flounder under black and white camouflage conditions. Coincident spectra were obtained with an ASD Spectrometer to compare spectra retrievals with the imager. (Dierssen)

l) Identified a new biological model for polarocrypsis (the Lookdown fish, *Selene vomer*) that is capable of reducing the polarization contrast against the dynamic polarization light field in near surface conditions under a range of solar azimuth and viewing angles (Cummings).

m) Field tested the Lookdown as a "polarocryptic" model for camouflage in the open ocean, near-surface environment in August 2011 (Cummings, Sullivan, Twardowski, Gilerson, Dierssen).

n) Characterized chromatophore responses to direct electrical stimulation and determined the effects of tetrodotoxin, a highly specific toxin that blocks axonal sodium channels in squid (Gilly)

o) Identification of distinct organizations and distributions of iridophores in species occupying different optical environments, including Lookdown (*Selene vomer*) in the open ocean, near-surface dwelling and Pinfish (*Lagodon rhomboides)* in the seagrass (Cummings)

p) Development of *in vitro* model systems to analyze iridophore and melanophore responses to molecular signals released from the nervous system (Cummings)

q) Further characterized the single scattering properties (Muller matrix and Extinction matrix) of an iridosome using first-principle simulation (DDA) (Kattawar)

r) Completed a full vector Monte Carlo code for fixed oriented particles. Incorporated the complex dependency of the extinction cross section on both incident angle and polarization state (through extinction matrix) in the simulation. (Kattawar)

s) Presented at MURI review in Arlington, VA in August 2010 (Cummings)

RESULTS

1. Detailed comparison of measured and modelled polarization characteristics of light (degree and angle of polarization) in the open ocean near surface environments (Fig. 1) (Gulf of Mexico campaign from June, 2010). Radiative transfer code based on Inherent Optical Property (IOP) measurements made at two sites under various sun conditions, azimuth orientations, depths and wavelengths showed almost perfect match to Stokes vector polarimetry measurements (Yu et al., *Applied Optics*, August 2011). Success suggests opening broader possibilities for simulations and validation by polarimetry and simulation modelling. (Kattawar, Gilerson, Sullivan, Twardowski, Dierrsen, Ahmed, Cummings)

2. Developed polarization technique for the retrieval of the index of refraction and particle size distribution of in water particulates based on the measured polarized reflectances and in water IOPs (Tonizzo et al., *Applied Optics, August 2011*). (Fig. 2,3) (Gilerson)

3. Quantified IOPs for all Florida Keys environments (MURI field campaigns - Jan. and Aug. 2011). The IOPs varied from values typical of open ocean "blue water" to turbid coastal "green water". Surprisingly, the VSF phase functions were relatively consistent, however the VSF magnitude varied over a large range. The Degree of Linear Polarization (DoLP) over all environments ranged from ~ 0.45 to 0.7 at a peak angle between 95 to 98° (Fig. 4). (Sullivan)

4. Developing methods using image analysis to estimate composite large-scale benthic reflectance from point spectral reflectance measurements of individual components (Fig. 5). (Dierssen)

5. Quantified and characterized the unique Polarocryptic response of the lookdown, *Selene vomer* (Fig 6) . The Lookdown exhibits a 21- 57% gain in polarocrypsis in the near surface, open ocean environment with a solar elevation of 60° across a full range of predator viewing angles (360°) than the conventional standard for crypsis in this environment, vertical mirrors (Fig 7). (Cummings)

6. Identified unique iridophore organization layers between marine fish species inhabiting different optical environments (Lookdown (*Selene vomer;* open ocean, near-surface dwelling*)* and Pinfish (*Lagodon rhomboides;* seagrass fish) have been examined to determine the organization of the iridophore layers in these species(Fig 8). (Cummings)

7. Hyperspectral imaging of the Sargassum crab, *Portunus sayi*, reveals excellent spectral matching to *Sargassum* across the visible spectrum, except for in the far red region of the spectrum (Fig. 9). Coloration of the crab appears to also have a diel periodicity that is being investigated further. For video of this research: http://www.youtube.com/watch?v=ygkO45QaMAw. (Dierssen)

8. Characterized iridophore and chromatophore responses to different neurotransmitters in the neon tetra and our other species of ecological interest (Fig 10). (Cummings)

9. Responses from electrically stimulated squid chromatophores (Fig. 11). supports the hypothesis that there are both central and peripheral pathways for chromatophore control. The peripheral pathway exists within the skin and appears to be distributed and autonomous in nature, or at least not under direct excitatory neural control. We propose that this peripheral control pathway is responsible for the irregular, flickering wave-like activity previously reported in free swimming squid. (Gilly)

10. Properties of the Mueller matrix and extinction matrix for a single iridosome were shown to depend on the incident wavelength, direction and polarization state (submitted to J*ournal of Royal Society Interface,* 2011). Comparing the Muller matrix patterns of an iridosome (layered cylinder) and a solid cylinder with same dimensions, we showed the sensitivity of scattering properties to their inner structures (Fig 12). This provides the basis for further multiple scattering simulation, and a reference for material scientists to emulate similar scattering properties. (Kattawar)

11. The considerations of the dependency of the extinction cross section on both incident direction and polarization state are necessary to give accurate Monte Carlo simulation for fixed orientation particles (Fig 13 b and c). The diffuse reflection spectrum of a layer of iridosomes is found depending on the incident direction (Fig 14), thus can be used to predict the color appearance of the animal. This code also enables us to calculate iridosome's optical response with arbitrary orientation distributions, and can be used as a part in the full 3D simulation of complex skin structures of both fish and cephalopods. (Kattawar)

IMPACT/APPLICATIONS

1. Success of our code suggests opening broader possibilities for simulations and validation by polarimetry and simulation modelling.

2. Identification of a new biomimicry model (the Lookdown, *Selene vomer*) for polarocrypsis, and our elaboration of the physical mechanisms underlying the model, will facilitate the development of new camouflage technologies/materials for use for naval operations.

3. Identification of ecologically-specific morphological structures for background matching suggests that effective underwater camouflage strategies and technologies will need to incorporate dynamically adaptable materials for movement into different optical zones.

4. Identification of two distinct neural control pathways (centralized and peripheral) for chromatophore movements suggests that an analogous heirarchical control strategy should potentially be employed for the development of a nanotechnology-based polarocryptic materials technology.

5. Development of computational-electrodynamics codes allowing the accurate modeling and performance optimization of dynamic birefringent multilayer structures, such as are found in teleost irridophores, is expected to enable the identification of new device structures of potential application to optoelectronics and communications technologies.

RELATED PROJECTS

(Gilly) Similar experiments were also carried out on California market squid (*Doryeuthis = Loligo opalesens*) at Hopkins Marine Station, but spontaneous propagating responses in this species are extremely rare, making it impossible to compare results with those in *Dosidicus*.

(Cummings, Kattawar) Acquired funding for the development of an integrated high-resolution and high speed polarizating imaging sensor for marine mooring deployments (Sept. 2011- Sept. 2014).

REFERENCES

Twardowski, M.S., E. Boss, J. B. Macdonald, W. S. Pegau, A. H. Barnard, and J. R. V. Zaneveld. (2001) "A model for estimating bulk refractive index from the optical backscattering ratio and the implications for understanding particle composition in case I and case II waters," Journal of Geophysical Research-Oceans 106, 14129-14142.

PUBLICATIONS

You, Y., A. Tonizzo, A. A. Gilerson, M. E. Cummings, P. Brady, J. M. Sullivan, M. S. Twardowski, H. M. Dierssen, S. A. Ahmed, and G. W. Kattawar. (2011) “Measurements and simulations of polarization states of underwater light in clear oceanic waters,” *Applied Optics*, 50, 4873-4893.

Tonizzo, A., A. Gilerson, T. Harmel, A. Ibrahim, J. Chowdhary, B. Gross, F. Moshary, and S. Ahmed. (2011) “Estimating particles composition and size distribution from the polarized water-leaving radiance,” *Applied Optics*, 50, 5047-5058.

Ibrahim, A., T. Harmel, A. Tonizzo, A. Gilerson, S. Ahmed.(2011) “Exploring the relation between polarized light fields and physical-optical characteristics of the ocean for Remote Sensing applications, “Proc. of SPIE, 8160.

Tonizzo, A., A. Gilerson, T. Harmel, A. Ibrahim, J. Chowdhary, B. Gross, F. Moshary, S. Ahmed. (2011) “Estimating particles microphysics from the polarized water-leaving radiance,” Proc. of SPIE, 8160.

Tonizzo, A., T. Harmel, A. Ibrahim, A. Gilerson, S. Ahmed. (2011) “Estimation of the attenuation coefficient of the water body using polarimetric observations,” Proc. of SPIE 8030: Ocean Sensing and Monitoring III, Weilin W. Hou; Robert Arnone, Editors.

Mcpherson, M., V.J. Hill, R.C. Zimmerman, and H.M. Dierssen. (2011) The optical properties of Greater Florida Bay: Implications for seagrass abundance. *Estuaries and Coasts.* DOI: 10.1007/s12237-011-9411-9.

Twardowski, M. S., X. Zhang, S. Vagle, J. Sullivan, S. Freeman, H. Czerski, Y. You, L. Bi, and G. Kattawar. (*in press*) The optical volume scattering function in the surf zone at Scripps Pier, CA with inversion to derive particle subpopulations, *J. Geophys. Res.*.

Sullivan, J. M., .M. S. Twardowski, J. R. V. Zaneveld, and C. C. Moore (*in press*): Measuring optical backscattering in water. *Light Scattering Reviews, Vol 7*.

Dierssen, H.M., Randolph, K. *Submitted*. Remote Sensing of Ocean Color. Encyclopedia of Sustainability Science and Technology. Springer-Verlag.

Dierssen, H.M. *Submitted*. Bathymetry. Encyclopedia of Natural Resources. Taylor & Francis Group.

Aurin, D. and H. M. Dierssen. *Submitted*. Remote sensing requirements for the optically complex waters of Long Island Sound. *Remote Sensing of the Environ*.

Meng G, Y. You, P Yang, and G. W. Kattawar. *Submitted*. Single Scattering Properties of Cephalopod Iridosomes. *Journal of the Royal Society Interface* (JRSI)

HONORS/AWARDS/PRIZES

"Distinguished Texas Scientist" for 2011 presented by the Texas Academy of Science (Kattawar)

FIGURES

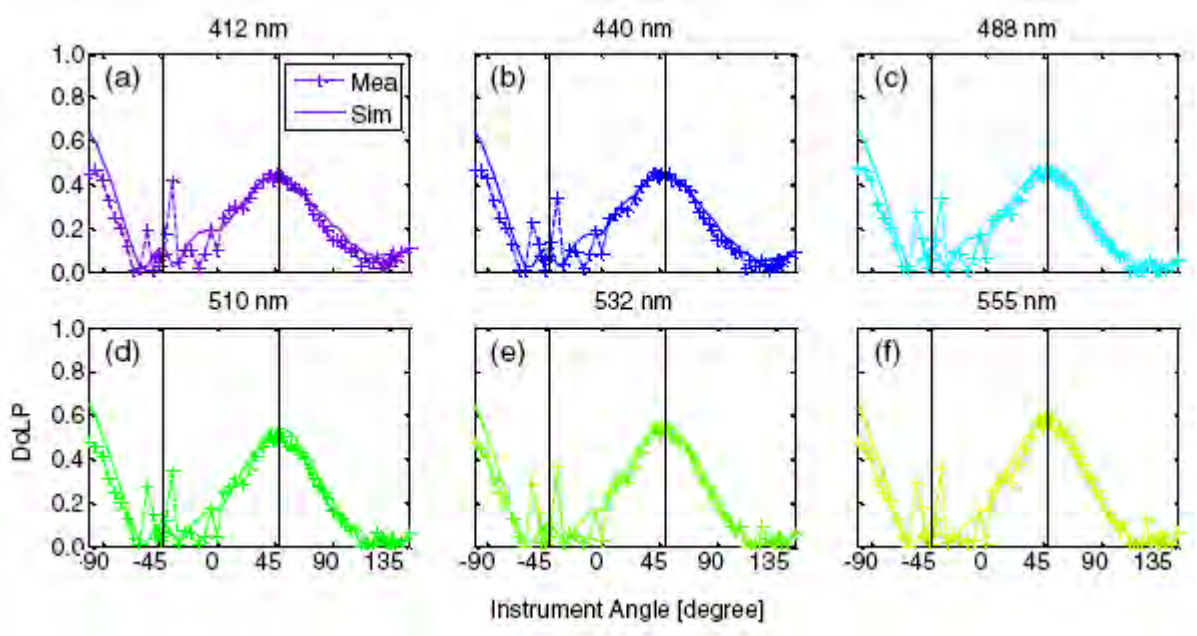

Figure 1. DoLP patterns from CCNY measurements and from simulations at ac-9 wavelengths for one of the stations, sun elevation 17.8°, main plane, depth =1m; the vertical line near 45° indicates the angle that corresponds to a 94° scattering angle; the vertical line near -45° indicates the edge of Snell's window, with angles within the window to its left.

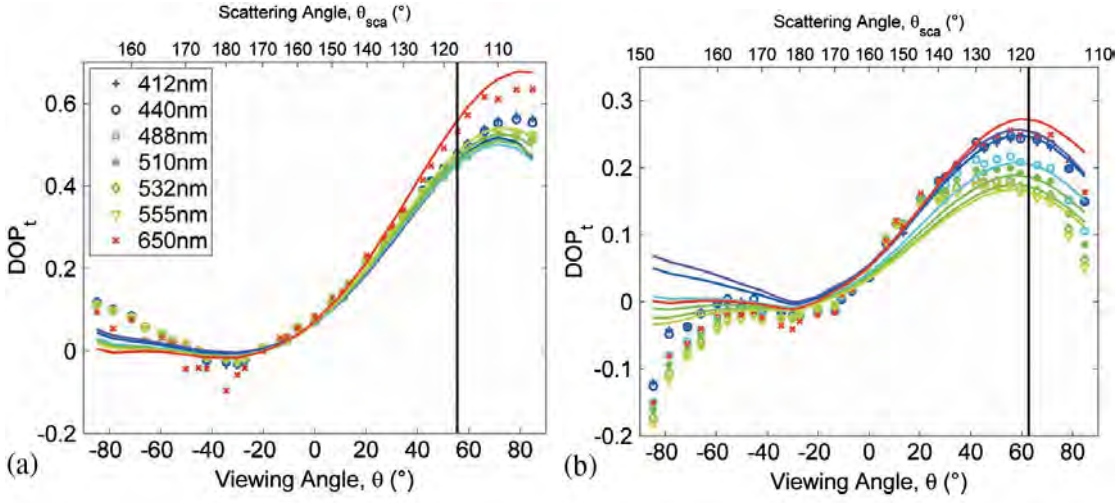

Figure 2. Total DOP_t vs. viewing angle and scattering angle for well retrieved index of refraction and PSD slope. (a) Case I, (b) Case II-Coastal. The vertical black line indicates the position of the specular reflection of sunlight. Computations are the solid lines. Tonizzo et al. (2011) Applied Optics.

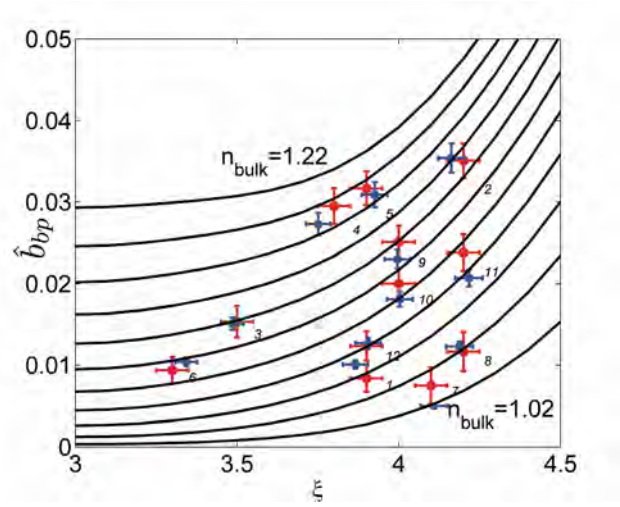

Figure 3. The backscattering ratio as a function of the hyperbolic slope of the particle size distribution. The solid black curves are results of Mie theory calculations, and each curve represents a different bulk refractive index (between 1.02 and 1.22, at steps of 0.02), from Twardowski et al., 2001 The blue squares are the estimated values using this paper (Twardowski et al., 2001) approach, the red circles are the estimated values obtained using polarimetric measurements. Tonizzo et al. (2011) Applied Optics.

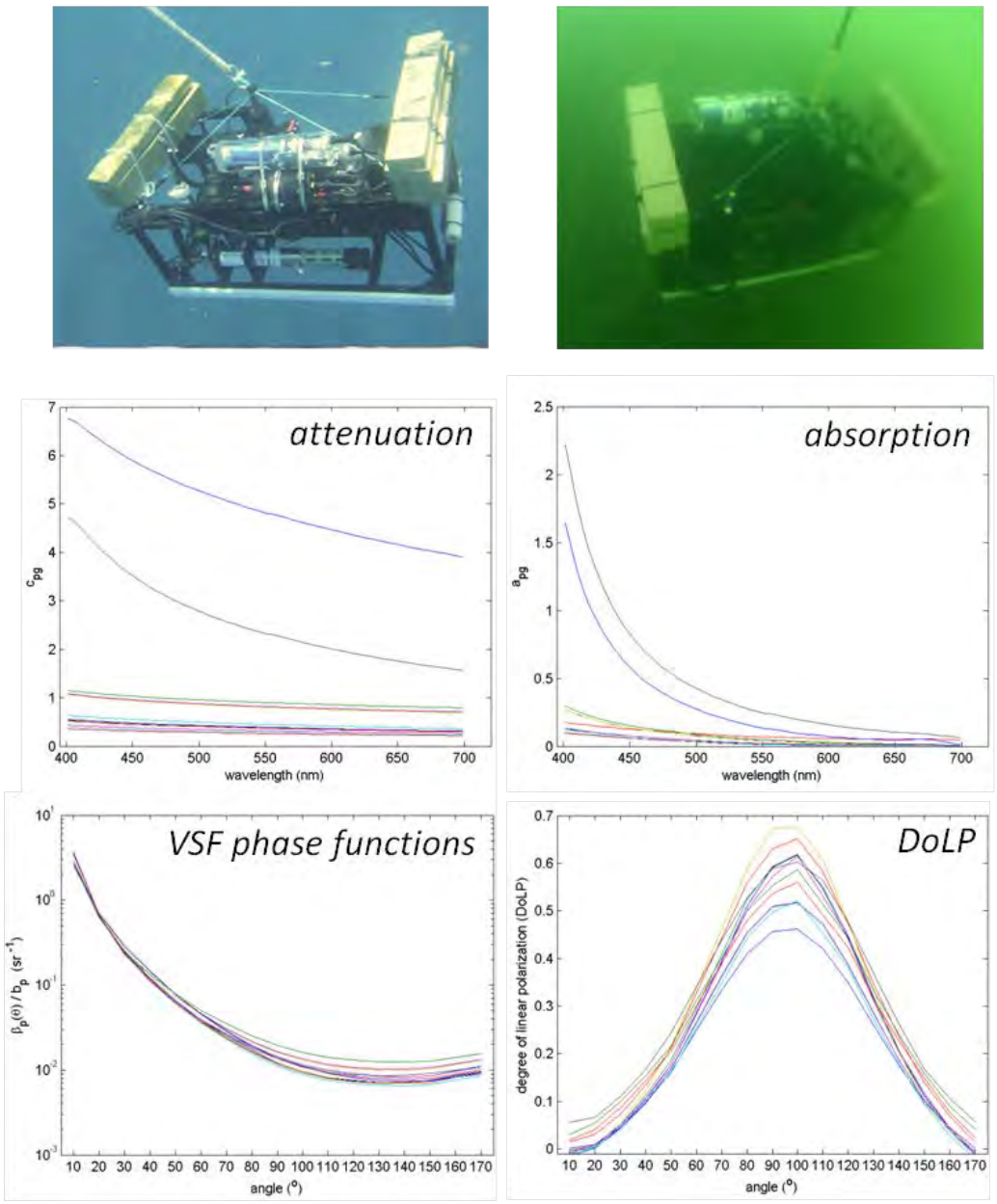

Figure 4. Variability in IOPs for all Florida Keys environments (MURI field campaign - Jan. 2011). The top panels show a visual example of the range of water clarity and color at the FL field sites (MASCOT package photographed underwater). The IOPs varied from values typical of open ocean "blue water" to turbid coastal "green water". Surprisingly, the VSF phase functions were relatively consistent. The Degree of Linear Polarization (DoLP) over all environments ranged from ~ 0.45 to 0.7 at a peak angle between 95 to 98°.

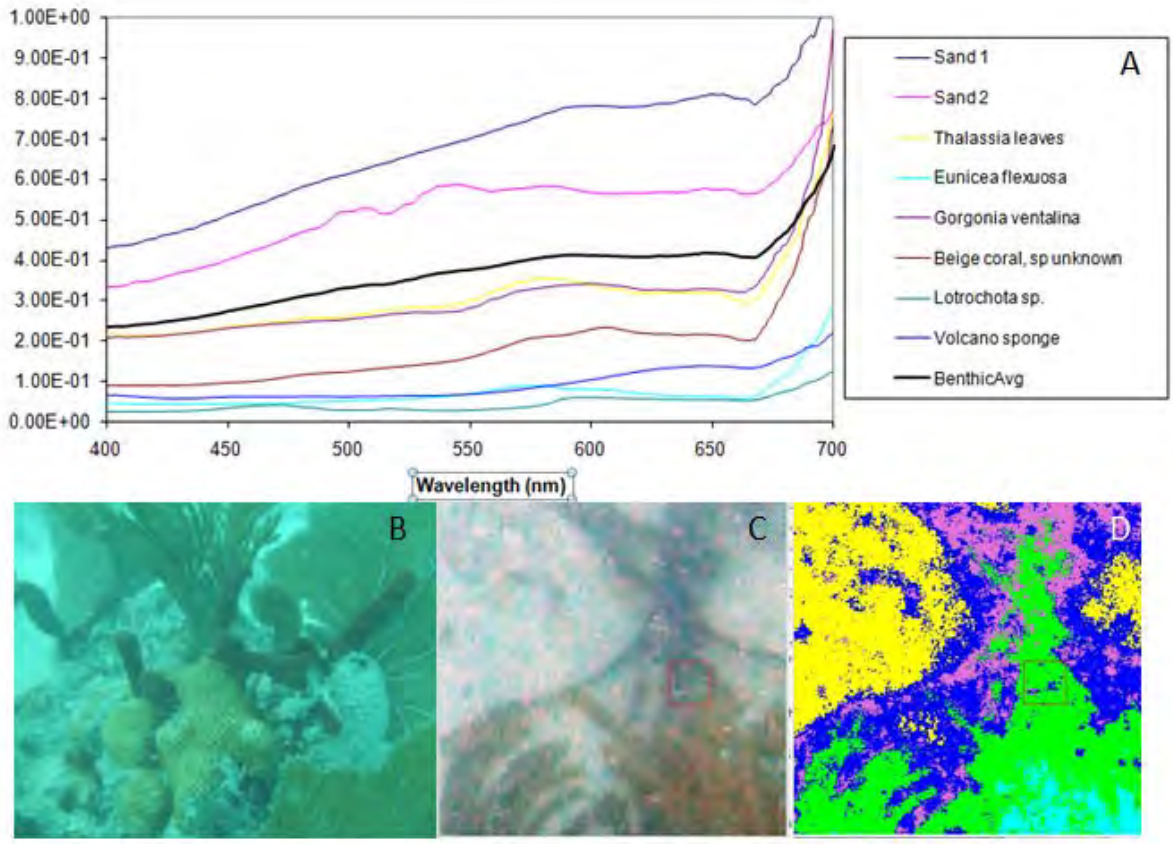

Figure 5. A) Benthic reflectance measurements of individual components at a station from greater Florida Bay. B) Oblique photograph of the individual benthic constituents at the station. C) Downlooking RGB image of the benthic constituents beneath the radiometer package; D) Classified image of the different benthic features used in the composite Benthic Reflectance measurement.

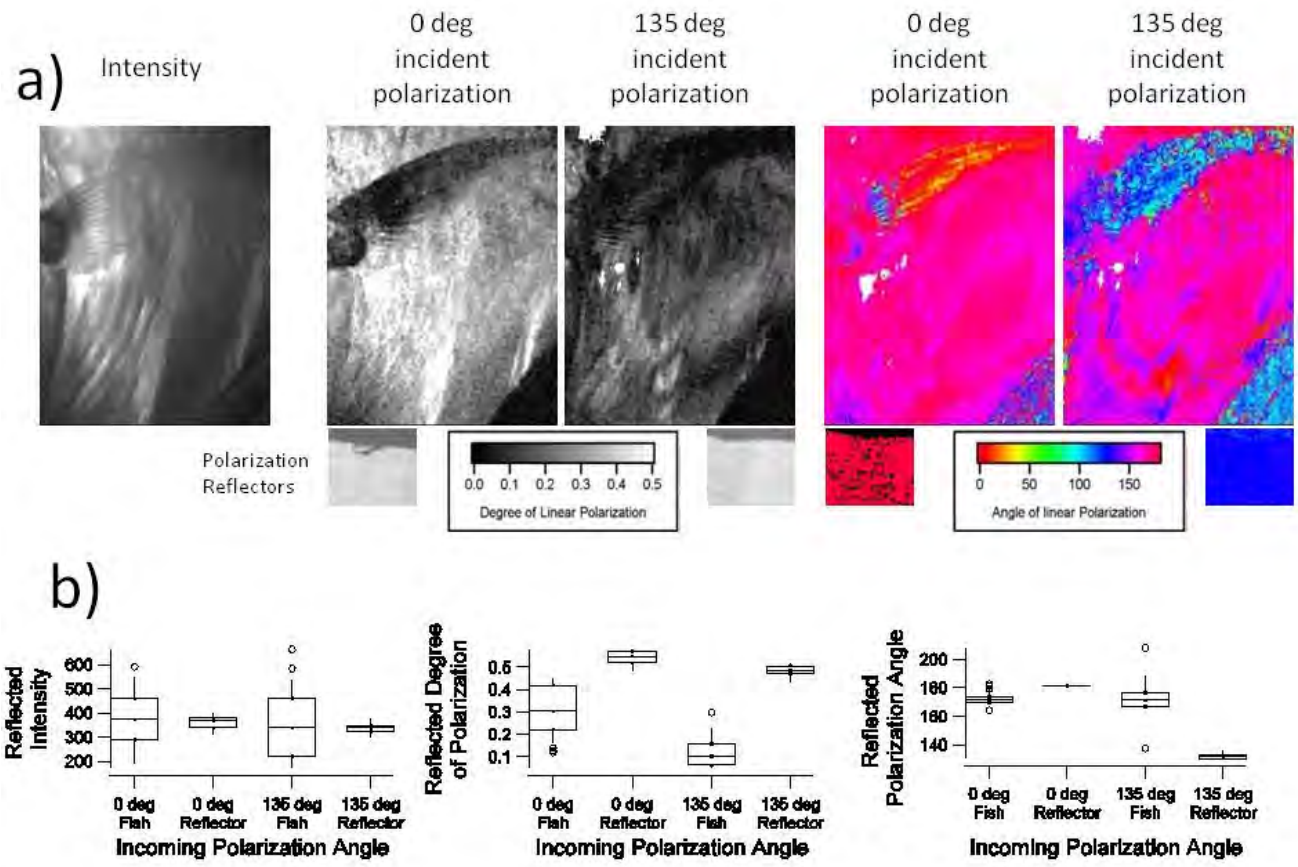

Figure 6. (a) We measure the polarization reflectance of the Lookdown, Selene volmer, under various incident polarization illuminations using a customized experimental tank. We show intensity, degree of linear polarization and angle of polarization data from our video polarimeter. (b) Box plots from 4 live Lookdowns relative to a mirror reflector show that the degree (t=7.3, p=3.2e-10) and angle (t=-24, p=9.7e-25) of linear polarized light varies significantly between the Lookdown and a vertical mirror at specific incident polarized light fields, while the intensity of reflectance does not (t=0.38, p=0.71). Specifically the degree of polarization significantly decreases when impinged upon by 135° polarized light (t=8.2, p=1.3e-11). The angle of polarization also behaves differently than a mirrored reflector. Both the mirror reflector and the Lookdown reflect horizontal polarized light (0° or 180°) under incident horizontal polarization illumination (0°), however, the Lookdown does not reflect incident 135d polarization illumination in conditions where an idealized reflector does. Such differential polarization reflectance is advantageous for near-surface background matching (see Figure 7).

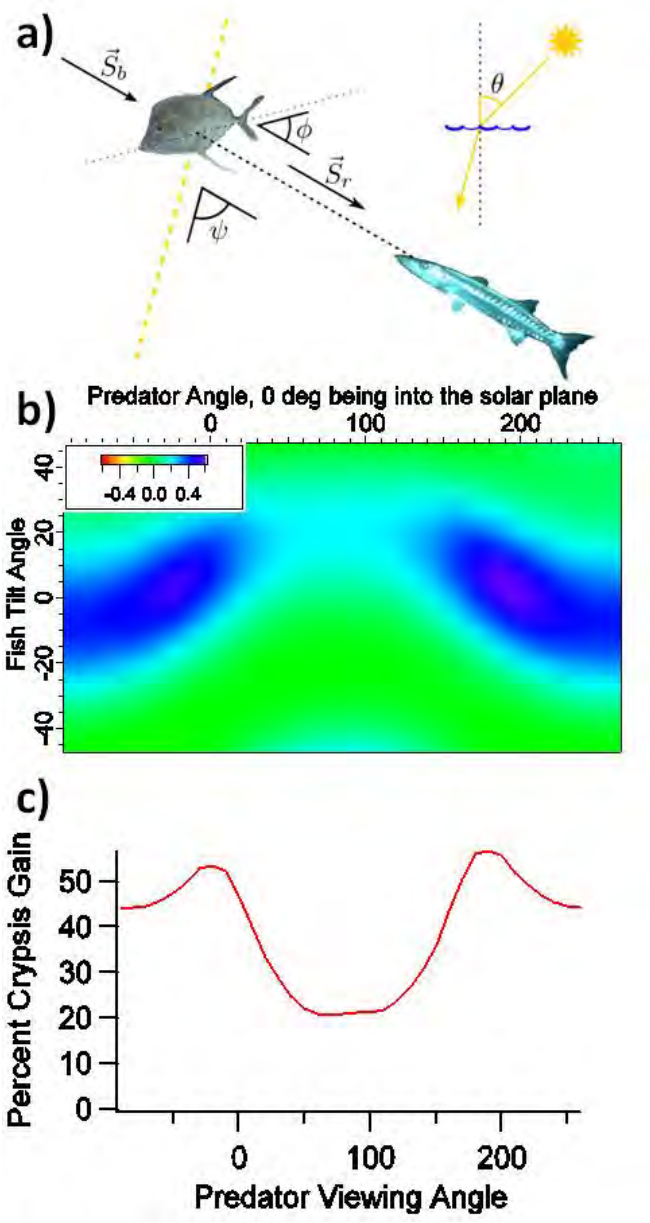

Figure 7. We model the polarization reflections of the fish using Mueller matrices measured from the Lookdown (See Fig 6). We evaluate polarocrypsis as the contrast ratio or the RMS difference between the target reflected Stokes vector (S_r) and the background Stokes vector (S_b) at solar elevation of $\theta = 60°$. (a) Three angles parameterize the contrast ratio calculation: θ, the angle between the sun and the zenith which defines the solar plane (indicated by the dotted orange line in the figure); ψ, the predator's observation angle with respect to the solar plane; and φ, the angle between the surface of the prey and the predator's observation angle. (b, c) We calculate the percent crypsis gain ($PG = 100 \times (G_{Lookdown} - G_{verticalmirror}) / G_{verticalmirror}$) between an idealized mirror and the lookdown fish Mueller matrix, where $G = \left\| \vec{S}_b - \vec{S}_r \right\|^{-1}$. We assume that the Mueller matrix rotates roughly invariantly with the angle φ, as our measurements indicate this to an approximation. (b) Percent crypsis gain (PG) across a range of fish tilt angles (-45° to 45°) for all possible predator viewing angles (ψ= 0° to 360°). (c) the PG for the optimal fish tilt from (b).

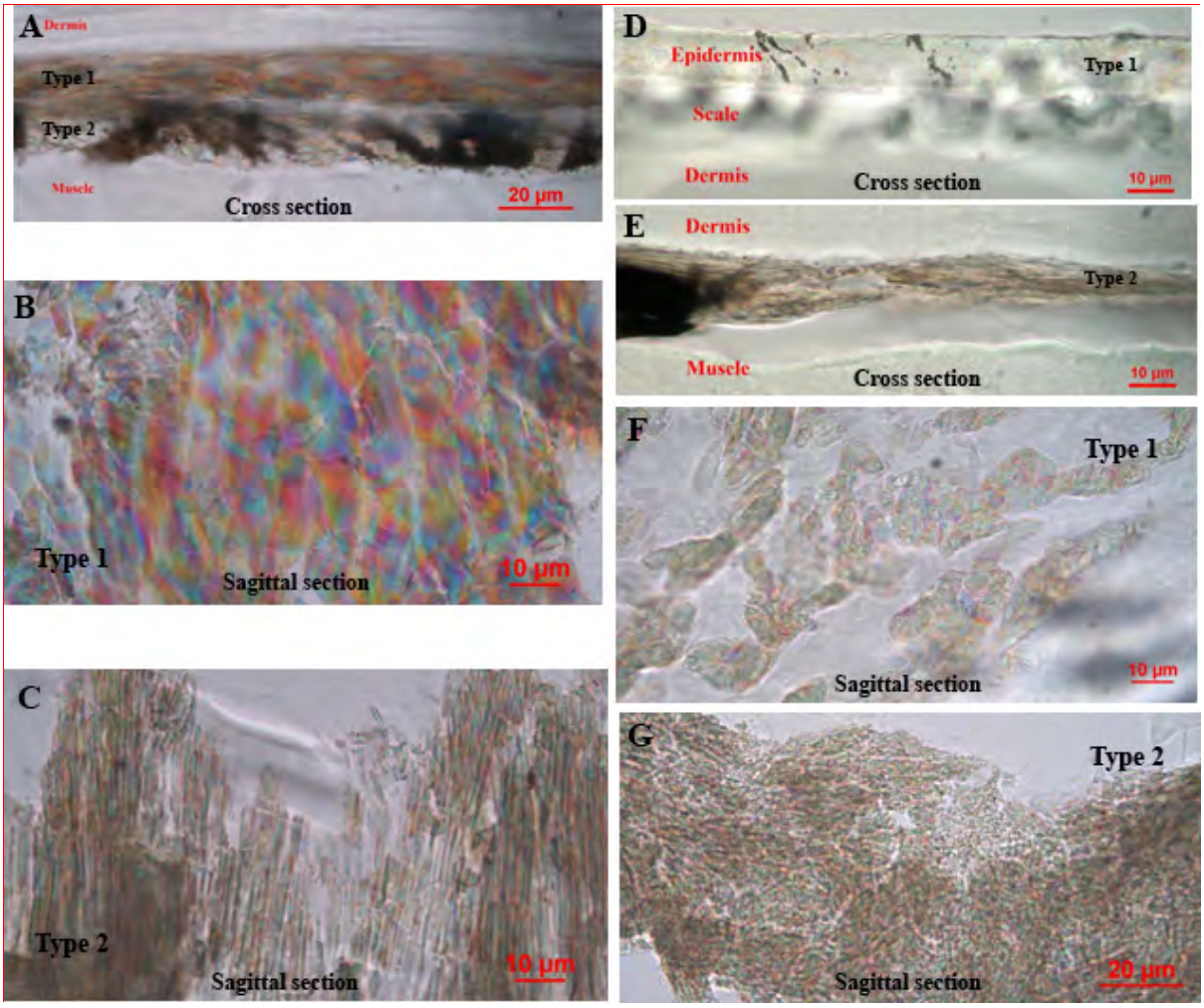

Figure 8. Two types of iridophores were observed in the skin of the open, ocean inhabiting Lookdown (A-C) and the shallow, seagrass inhabiting Pinfish (D-G). A, D and E are cross sections and the rest of images are sagittal sections. In Lookdown, both iridophore types are present in the dermis and type 2 iridophores lie just underneath the type 1 iridophore layer (A). Melanophores appear to be associated primarily with type 2 iridophores (A). Type 1 iridophores have relatively large guanine platelets (approximate dimension 5 µm x 20 µm; see B) while type 2 iridophores have small and thin guanine platelets (approximate dimension 1 µm x 10 µm) and are very densely packed (C). In the pinfish, the type 1 iridophores are located in the epidermis (D) while the type iridophores in the dermis (E). The type 1 iridophores have relatively large guanine platelets with an approximate dimension of 5 µm x 12 µm (F). The type 2 iridophores have small and short guanine platelets (approximate dimension 0.8 µm x 2.5 µm) (G).

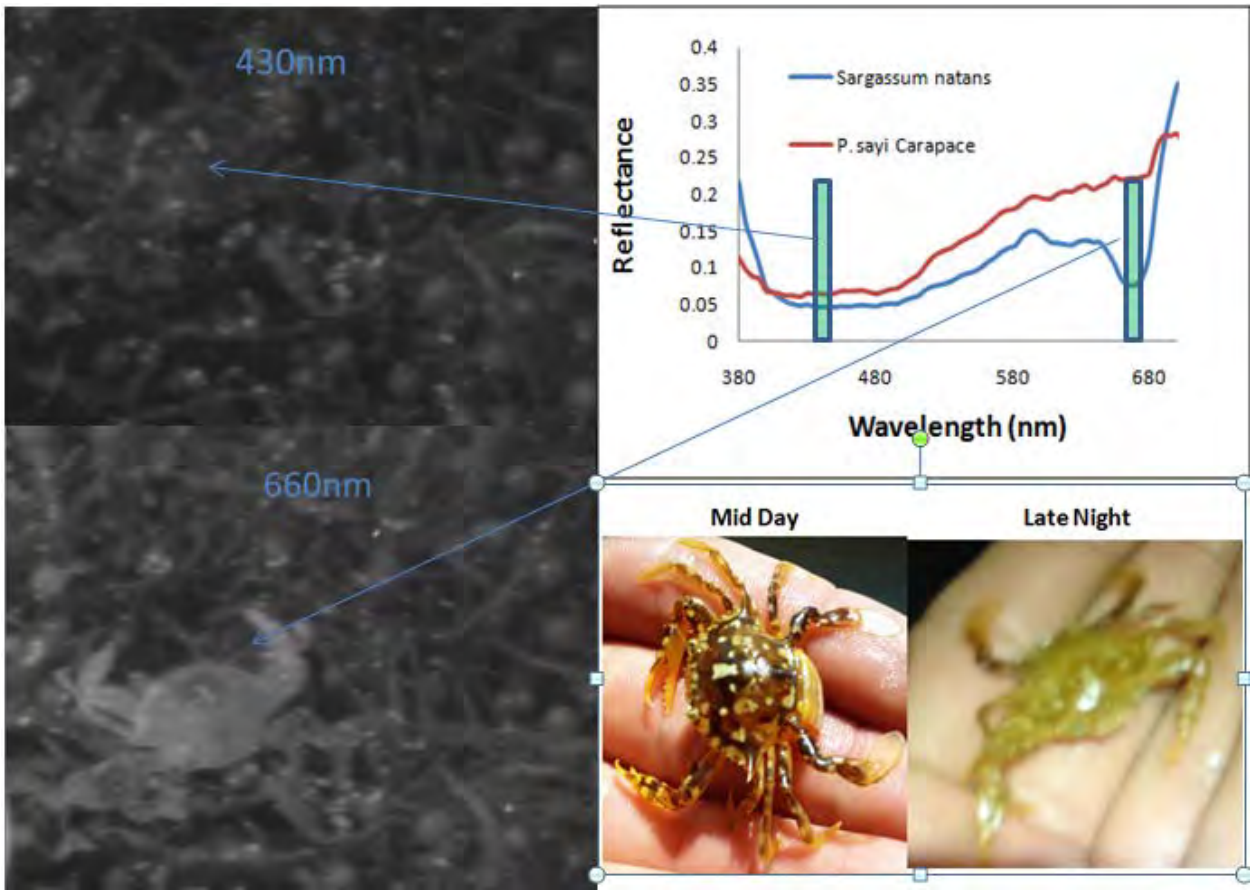

Figure 9. Imaging of the Sargassum crab, Portunus sayi, shows A) the crab is completely cryptic in the Sargassum algae at 440 nm, B) compared to 660 nm where the crab becomes visible. C) Spectral reflectance signature measured with 710 imager of the crab in comparison to the Sargassum. D) Diel variability in crab coloration is being investigated in controlled laboratory experiments.

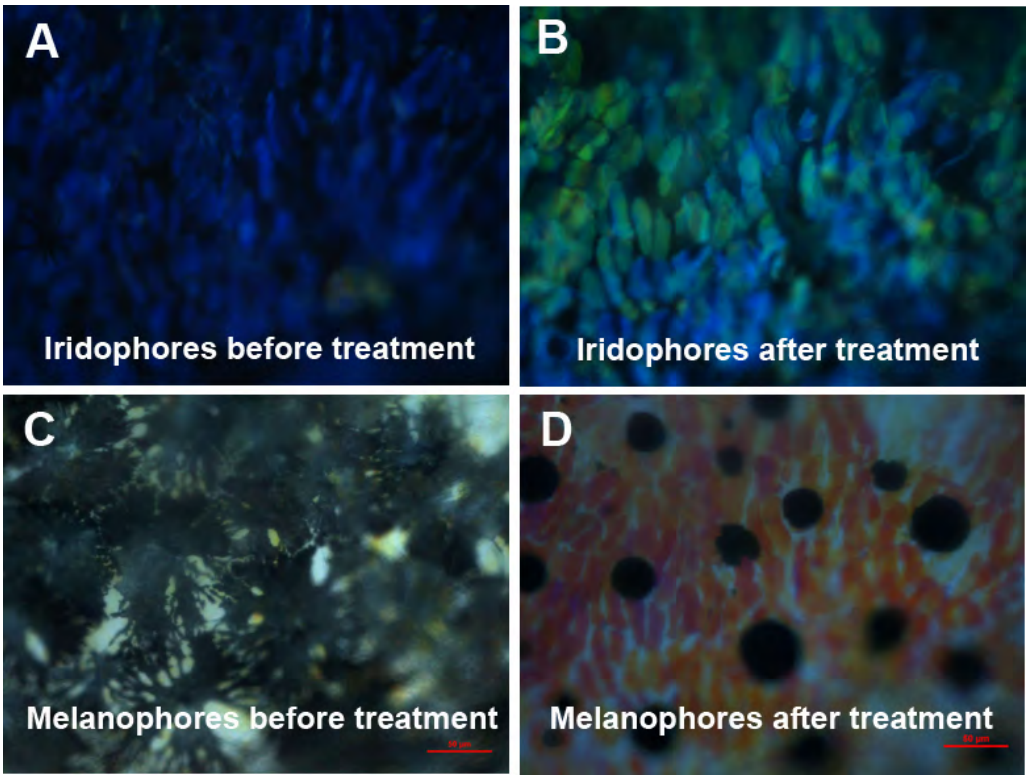

Figure 10: A skin preparation from neon tetra was placed in the flow chamber with Ringer's buffer containing 2.7 mM KCl. Iridophores appared as blue under epi-illumination (A). After Ringer's buffer with 50 mM KCl (but with the same osmolarity) was infused into the flow chamber, the iridophores gradually became green-yellow in 5-10 minutes (B). Melanophores were initially in dispersed state and iridophores were masked by melanophores (C; transmitted illumination was used). After the treatment with 50 mM KCl, melanophores aggregated and stacks of guanine platelets in iridophores were seen as pink or yellow (D). Similar effects were observed when norepinephrine were used as stimulation.

(a)

(b)

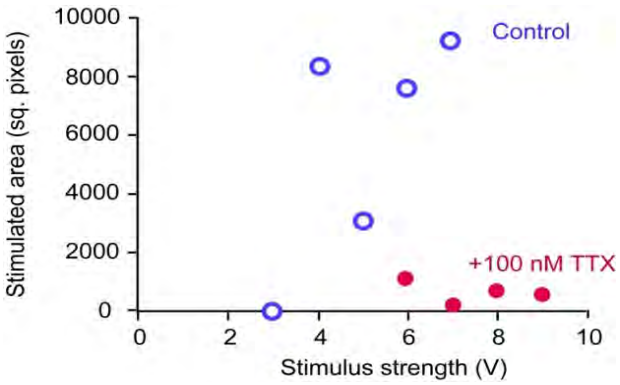

(c)

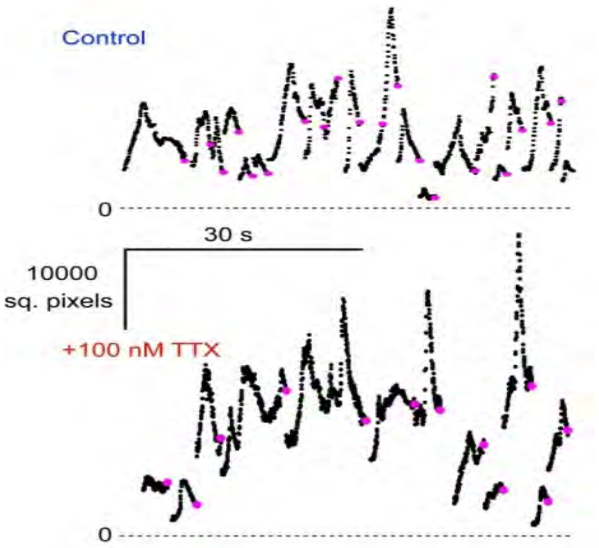

Figure 11. (a) Preparation of a piece of excised Dosidicus fin (2 x 4 cm) positioned ventral-side up for chromatophore stimulation experiments. The tip of the coaxial, bipolar stimulating electrode is in the center of the frame. Stimulating pulses were 1 ms duration and typically 3-10 V amplitude. Experiments were carried out at room temperature of 20-22 °C. (b) Effect of TTX on stimulated chromatophore activity. Addition of TTX (100nM) essentially blocked all stimulated activity. Results are typical of 6 experiments. (c) Effects of TTX on spontaneous, propagated chromatophore-activity. Individual events end at the purple dots and have been concatenated, i.e., variable amounts of time have been omitted between events. This type of spontaneous event persisted in the presence of 100 nM TTX with no noticeable change in amplitude or frequency.

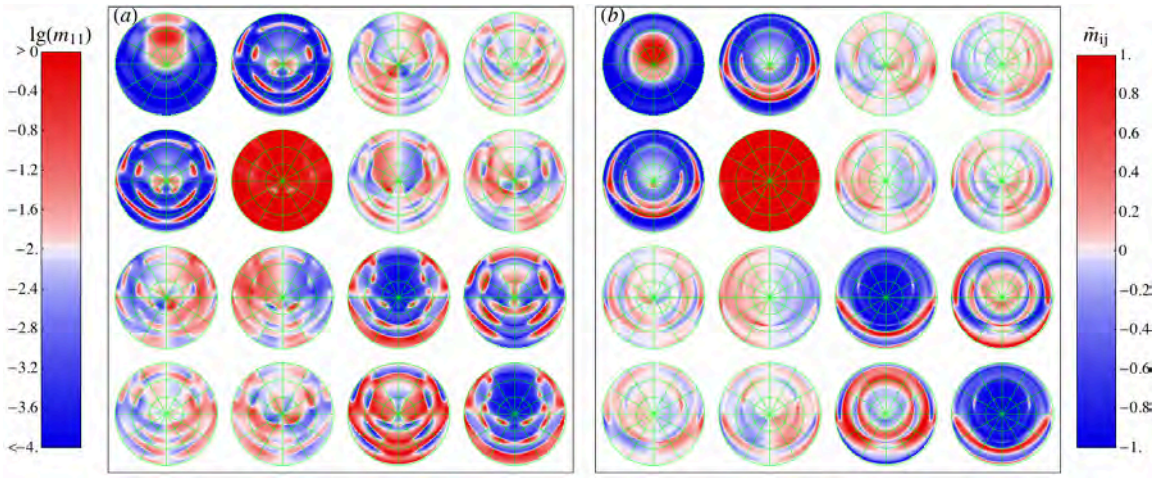

Figure 12. Angular distribution of the reduced backscattering Mueller matrix with incident angle β=30° and wavelength 0.48μm for (a) 5 layer iridosome (shown in Fig 13) with radius r=0.5μm, (b) solid cylinder with the same radius and total height. m_{11} plotted on a log 10 scale with the color bar on the left; the right color bar is for all other reduced Mueller matrix elements ($m_{ij,\ i\neq1,j\neq1}$).
(Submitted to Journal of Royal Society Interface, 2011)

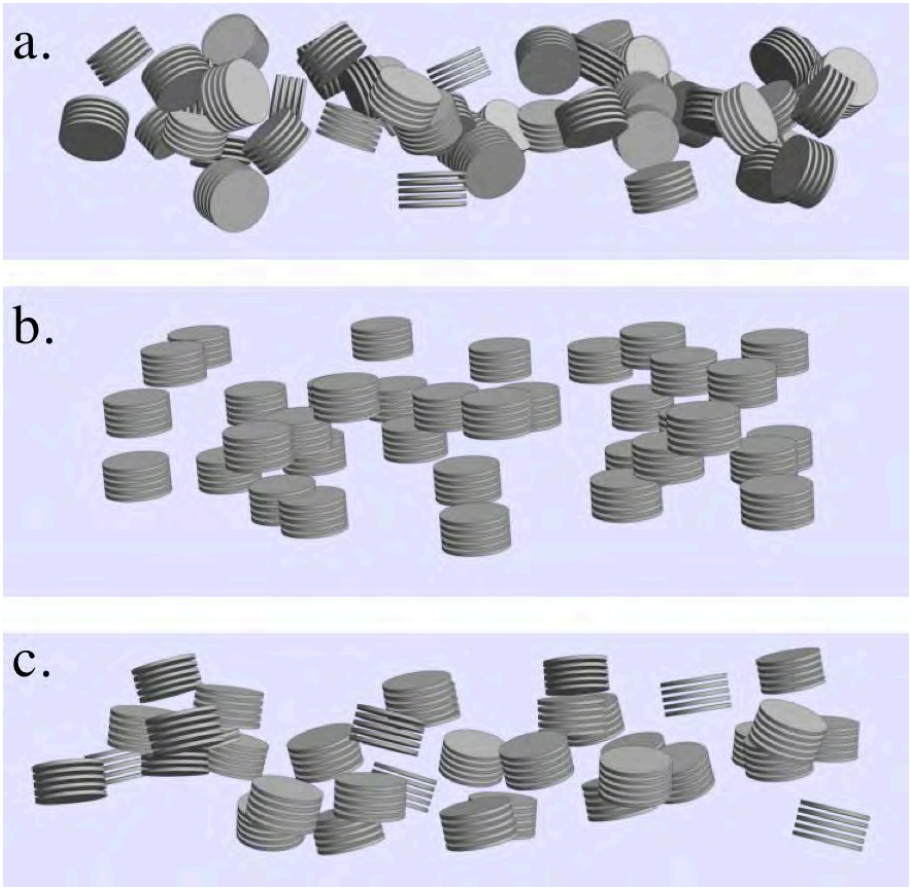

Figure 13. Illustrations of an iridosome system with (a) complete random orientations, (b) fixed orientations, and (c) partial random/fixed orientations.

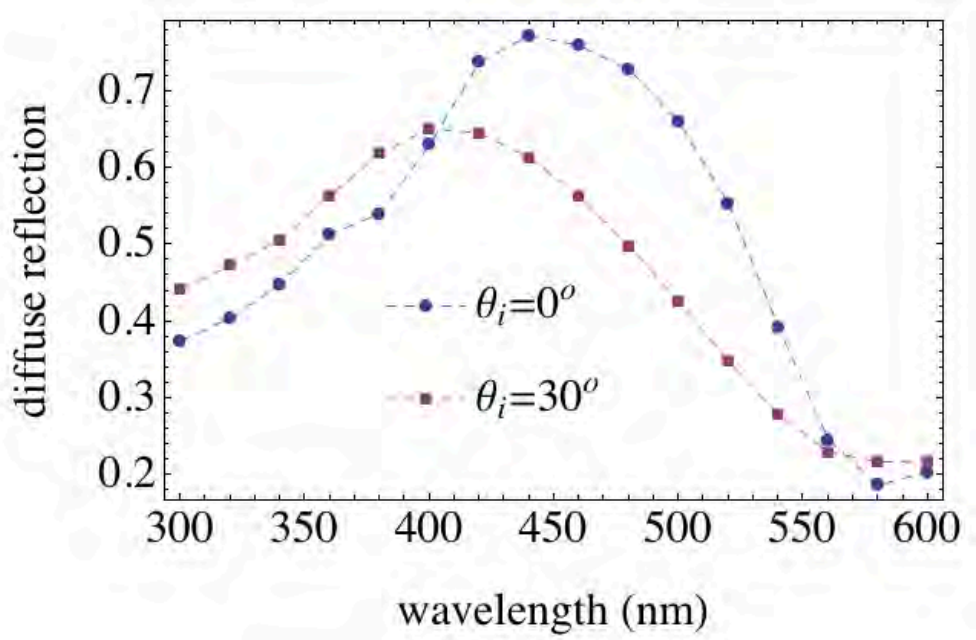

Figure 14. The diffuse reflection vs. incident wavelength (in water) and direction in a fixed oriented system (Fig 13.b). The reflection spectrum is shown depending on the incident angle, which can't be observed in a complete random oriented system (Fig 13.a). The realistic orientation distribution (similar to Fig 13.c) can be obtained from biological measurement.